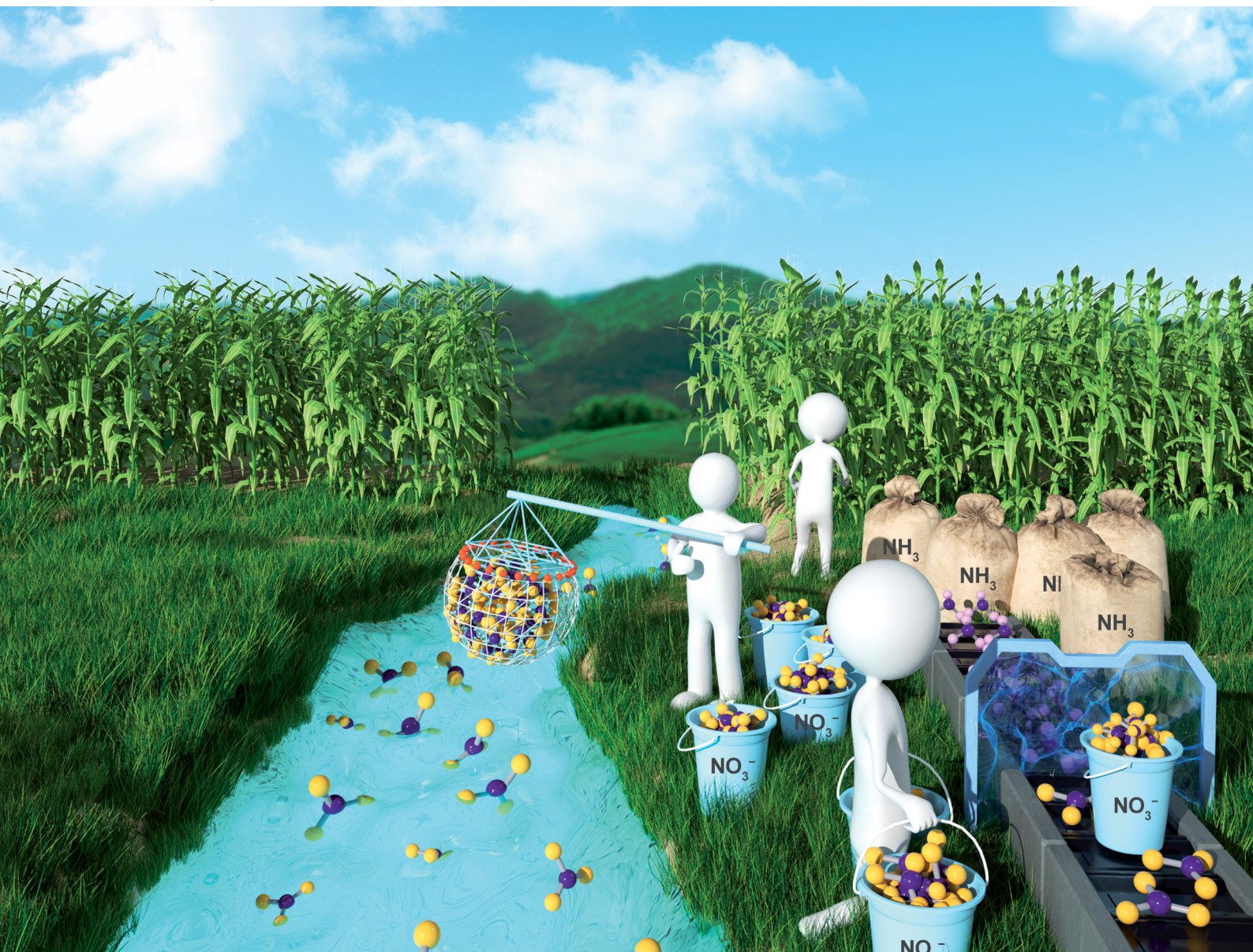


# EES Catalysis

rsc.li/EESCatalysis



ISSN 2753-801X

**PAPER**

Wenzhen Li, Shuang Gu *et al.*  
Sustainable waste-nitrogen upcycling enabled  
by low-concentration nitrate electrodiolysis and  
high-performance ammonia electrosynthesis



Cite this: *EES Catal.*, 2023,  
1, 504

## Sustainable waste-nitrogen upcycling enabled by low-concentration nitrate electro dialysis and high-performance ammonia electrosynthesis†

Yifu Chen,<sup>a</sup> Pouya Ammari-Azar,<sup>b</sup> Hengzhou Liu,<sup>a</sup> Jungkuk Lee,<sup>a</sup> Yu Xi,<sup>a</sup> Michael J. Castellano,<sup>c</sup> Shuang Gu<sup>\*b</sup> and Wenzhen Li<sup>\*a</sup>

Reactive nitrogen (Nr) is an essential nutrient to life on earth, but its mismanagement in waste has emerged as a major problem in water pollution to our ecosystems, causing severe eutrophication and health concerns. Sustainably recovering Nr [such as nitrate (NO<sub>3</sub><sup>-</sup>-N)] and converting it into ammonia (NH<sub>3</sub>) could mitigate the environmental impacts of Nr, while reducing the NH<sub>3</sub> demand from the carbon-intensive Haber–Bosch process. In this work, high-performance NO<sub>3</sub><sup>-</sup>-to-NH<sub>3</sub> conversion was achieved in a scalable, versatile, and cost-effective membrane-free alkaline electrolyzer (MFAEL): a remarkable NH<sub>3</sub> partial current density of 4.22 ± 0.25 A cm<sup>-2</sup> with a faradaic efficiency of 84.5 ± 4.9%. The unique configuration of MFAEL allows for the continuous production of pure NH<sub>3</sub>-based chemicals (NH<sub>3</sub> solution and solid NH<sub>4</sub>HCO<sub>3</sub>) without the need for additional separation procedures. A comprehensive techno-economic analysis (TEA) revealed the economic competitiveness of upcycling waste N from dilute sources by combining NO<sub>3</sub><sup>-</sup> reduction in MFAEL and a low-energy cost electro dialysis process for efficient NO<sub>3</sub><sup>-</sup> concentration. In addition, pairing NO<sub>3</sub><sup>-</sup> reduction with the oxidation of organic Nr compounds in MFAEL enables the convergent transformation of N–O and C–N bonds into NH<sub>3</sub> as the sole N-containing product. Such an electricity-driven process offers an economically viable solution to the growing trend of regional and seasonal Nr buildup and increasing demand for sustainable NH<sub>3</sub> with a reduced carbon footprint.

Received 16th March 2023,  
Accepted 21st March 2023

DOI: 10.1039/d3ey00058c

rsc.li/eescatalysis

### Broader context

The integrated sustainable process presented in this work provides an efficient approach to upcycling waste nitrogen, and it may be extended to CO<sub>2</sub> capture from various sources, thanks to the basicity of ammonia. The synergistic combination of CO<sub>2</sub> capture and ammonia synthesis may magnify the environmental benefits when adopted by real-world deployments. Owing to the flexibility and scalability of electrochemical systems, the distributed synthesis of green ammonia can also be realized from waste nitrogen sources, as opposed to the centralized synthesis of carbon-intensive methane-based ammonia manufacturing in Haber–Bosch plants. Findings on the conversion of organic nitrogen open up an alternative pathway for managing solid nitrogen-containing wastes for sustainable agriculture and the environment. The electro dialysis demonstrated for nitrate concentration can be adopted for the separation of other charged species in dilute sources, such as heavy metal removal and precious metal recovery. The established framework of the techno-economic analysis may be expanded to other electrolysis and electro dialysis systems. The unique ultra-alkaline NaOH/KOH/H<sub>2</sub>O system employed in this work may serve as an enabling electrolyte, inspiring other electrochemical conversions with tailored selectivity or activity.

## Introduction

As opposed to “inert nitrogen (N<sub>2</sub>)”, reactive nitrogen (Nr) is referred to as a variety of nitrogen-containing compounds that are active biologically, chemically, and/or photochemically. Nr is essential to life on earth as a basic building block of amino acids, proteins, nucleic acids, and other molecules necessary for life activities.<sup>1,2</sup> The global Nr generation has increased by ~70% over the past 30 years, >60% of which can be attributed to the anthropological N<sub>2</sub>-fixing process in the

<sup>a</sup> Department of Chemical and Biological Engineering, Iowa State University, Ames, Iowa 50011, USA. E-mail: wzli@iastate.edu

<sup>b</sup> Department of Mechanical Engineering, Wichita State University, Wichita, Kansas 67260, USA. E-mail: Shuang.Gu@wichita.edu

<sup>c</sup> Department of Agronomy, Iowa State University, Ames, Iowa 50011, USA

† Electronic supplementary information (ESI) available. See DOI: <https://doi.org/10.1039/d3ey00058c>



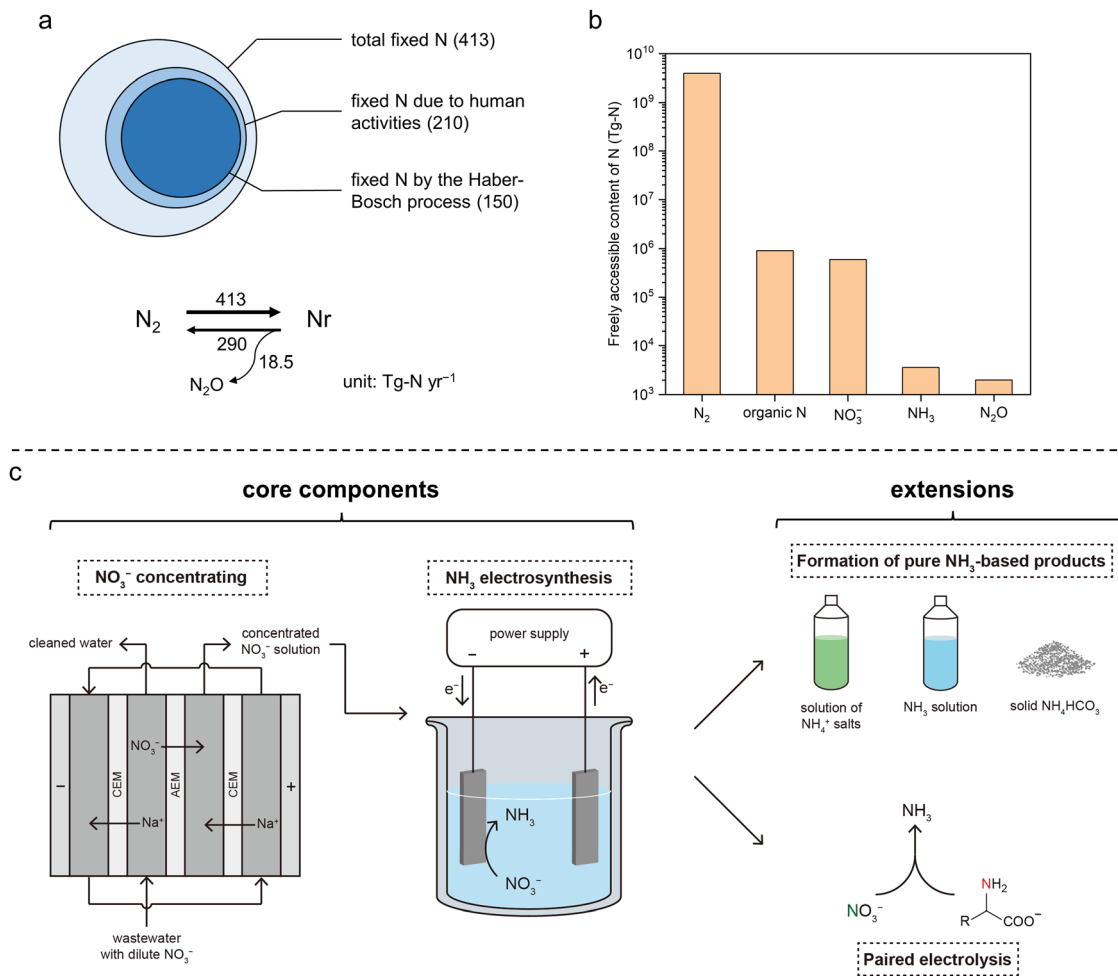
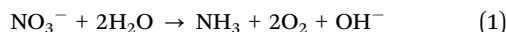


**Fig. 1** Global N balance, N accessibility, and the presented integrated sustainable process. (a) Simplified annual balance of the global N cycle. Top: Contribution of human activities to the fixation of N<sub>2</sub>. Bottom: Estimation of the rates of N<sub>2</sub> fixation (N<sub>2</sub> to Nr), denitrification (NO<sub>3</sub><sup>-</sup> to N<sub>2</sub>), and N<sub>2</sub>O generation accompanied by denitrification. The numbers are in teragrams of N per year (Tg-N yr<sup>-1</sup>) and were obtained from Ref. 5. (b) Estimated amounts of freely accessible N element in different forms in the global ecosystem. Data are obtained from Ref. 2. Organic N, NO<sub>3</sub><sup>-</sup>, NH<sub>3</sub>, and N<sub>2</sub>O are the four most abundant forms of accessible Nr. (c) Schematic of the integrated sustainable process for upcycling waste nitrogen in this work. The two core components are (1) NO<sub>3</sub><sup>-</sup> recovery from low-concentration waste streams by electrodes and (2) NO<sub>3</sub><sup>-</sup>-to-NH<sub>3</sub> conversion by electrolysis. Two extensions were also demonstrated, including the formation of NH<sub>3</sub>-based chemicals and paired electrolysis. Abbreviations: CEM, cation-exchange membrane; AEM, anion-exchange membrane.

industry [*i.e.*, the Haber-Bosch process for ammonia (NH<sub>3</sub>) synthesis] to fulfill the growing global food demand.<sup>3,4</sup> The microbial decomposition-nitrification-denitrification process can turn Nr back to N<sub>2</sub> in nature; however, the generation rate of artificial Nr species is far greater than the elimination rate of those Nr species by the natural process,<sup>5,6</sup> resulting in continued accumulation that has caused alarming and profound damage to the ecosystems as well as human welfare (Fig. 1a and Fig. S1a, ESI†).<sup>7</sup> For example, the excessive Nr in major U.S. rivers from fertilization of crop fields (fertilizer runoff) and from food processing facilities (waste discharge) has been firmly linked to the seasonal eutrophication of the coastal areas, including the formation of notorious “dead zones”.<sup>1</sup> In fact, most of the escaped Nr in the ecosystem ends up in the form of nitrate (NO<sub>3</sub><sup>-</sup>) because of its highest oxidation state. Excessive levels of NO<sub>3</sub><sup>-</sup>-N have been related to some severe health hazards, including birth defects, blue baby syndrome,

thyroid disease, and certain cancers if not properly treated in domestic water.<sup>8-10</sup> Therefore, restoring the balance between the generation and elimination of Nr (particularly, NO<sub>3</sub><sup>-</sup>-N) is an important and urgent task for us today.<sup>11</sup>

Sustainable solutions to this human-induced problem have been actively pursued in recent years, such as the electrochemical reduction of NO<sub>3</sub><sup>-</sup> (NO<sub>3</sub>RR). If NO<sub>3</sub><sup>-</sup> in waste streams can be efficiently recovered and converted to NH<sub>3</sub> (eqn (1)), this NH<sub>3</sub>-centric process will alleviate the environmental impacts of NO<sub>3</sub><sup>-</sup>, while substantially decreasing NH<sub>3</sub> demand from the Haber-Bosch process using fossil fuel-derived H<sub>2</sub>.<sup>12,13</sup>



Despite the successful development of some electrocatalysts for the NO<sub>3</sub><sup>-</sup>-to-NH<sub>3</sub> process in previous works (Table S1, ESI†),<sup>14-19</sup> many of them involve noble metals and/or require



complicated synthetic procedures, making them less economically attractive, especially considering the electricity consumption for this 8-electron-transfer reaction. Moreover,  $\text{NO}_3^-$  is highly distributed with only tens or hundreds of ppm  $\text{NO}_3^-$ -N in typical waste streams;<sup>12</sup> thus, an efficient and sustainable concentrating step is another prerequisite for the high-performance  $\text{NH}_3$  electrosynthesis. Nevertheless, a systematic assessment of the technical and economic feasibility of  $\text{NO}_3^-$  concentration is critically missing in the current research field.

In this work, we report an integrated electricity-driven process for economically upcycling waste  $\text{NO}_3^-$ -N enabled by low-concentration  $\text{NO}_3^-$  electro-dialysis and high-performance  $\text{NH}_3$  electrosynthesis from  $\text{NO}_3^-$  reduction (Fig. 1c). In a membrane-free alkaline electrolyzer (MFAEL) with a NaOH/KOH/ $\text{H}_2\text{O}$  as the robust electrolyte, an  $\text{NH}_3$  partial current density of  $4.22 \pm 0.25 \text{ A cm}^{-2}$  from  $\text{NO}_3^-$  reduction with a faradaic efficiency (FE) of  $84.5 \pm 4.9\%$  was achieved on a simple commercial nickel foam as the cathode material. Meanwhile, low energy consumption was demonstrated to recover  $\text{NO}_3^-$  from low concentration (7.14 mM, or 100 ppm  $\text{NO}_3^-$ -N) by efficient electro-dialysis for the first time. The economic competitiveness was quantitatively analyzed for the combined process of the  $\text{NO}_3^-$  recovery (by the low-concentration electro-dialysis) and the  $\text{NO}_3^-$ -to- $\text{NH}_3$  conversion (by the high-performance electrolysis), as compared to the prevailing treatment methods of waste nitrogen. As one extension of the integrated process, continuous production of pure  $\text{NH}_3$ -based chemicals ( $\text{NH}_3$  solution and solid  $\text{NH}_4\text{HCO}_3$ ) was realized without the need for additional separation procedures. As another logical extension, pairing  $\text{NO}_3^-$  reduction on the cathode with the oxidation of organic Nr compounds on the anode led to  $\text{NH}_3$  production from both electrodes simultaneously, realizing the convergent transformation of various Nr into  $\text{NH}_3$  as the sole N-containing product. The integrated process offers an all-sustainable and economically viable route for upcycling waste  $\text{NO}_3^-$ -N into the highest-demanded N-based chemical product –  $\text{NH}_3$ , so that the growing trend of regional and seasonal Nr buildup could be largely decelerated and reversed.

## Results and discussion

### High-rate $\text{NH}_3$ production by NO3RR in NaOH/KOH/ $\text{H}_2\text{O}$

With ultrahigh alkalinity, the “NaOH/KOH/ $\text{H}_2\text{O}$ ” electrolyte was first introduced in an attempt to convert  $\text{N}_2$  to  $\text{NH}_3$ , but the system was later confirmed to completely reduce  $\text{NO}_x^-$ -N even at a trace amount of  $\text{NH}_3$  on simple metal electrodes.<sup>20–22</sup> Such an unexpected finding implies that this strongly alkaline electrolyte holds potential for efficiently converting Nr into  $\text{NH}_3$  for the alternative upcycling of waste nitrogen.

Thermodynamic analysis performed in this work (Fig. S2, ESI†) clearly indicates that the reduction of  $\text{NO}_3^-$  to  $\text{NH}_3$  is much more favorable than the reduction of water (*i.e.*, the hydrogen evolution reaction, HER). Furthermore, the formation of gaseous  $\text{NH}_3$  is even more favorable than that of aqueous  $\text{NH}_3$  ( $\text{NH}_3 \cdot \text{H}_2\text{O}$ ) at temperatures greater than 30 °C. In addition,

if the produced  $\text{NH}_3$  can be removed timely from the reaction system (such as by a carrier gas flow), the thermodynamic cell voltage will be further reduced due to the shift in the chemical equilibrium.

Motivated by these results, we investigated the Nr-to- $\text{NH}_3$  conversion in the NaOH/KOH/ $\text{H}_2\text{O}$  electrolyte on simple nickel (mesh and foam) electrodes at a range of elevated temperature of 80–200 °C in a one-compartment MFAEL system (Fig. S3, ESI†). In the NaOH/KOH/ $\text{H}_2\text{O}$  electrolyte with a carefully-chosen composition (containing equimolar NaOH and KOH with 40 wt% of water), the  $\text{NO}_3^-$ -to- $\text{NH}_3$  conversion on simple Ni cathodes is surprisingly active: an  $\text{NH}_3$  partial current density of  $4.22 \pm 0.25 \text{ A cm}^{-2}$  was obtained with  $84.5 \pm 4.9\%$  of FE towards  $\text{NH}_3$  and  $82.0 \pm 0.2\%$  of  $\text{NO}_3^-$  conversion on a commercial nickel foam at 80 °C (Fig. 2a and Fig. S4a, ESI†). Despite the slightly lower faradaic efficiency and the mildly elevated temperature, such a remarkable  $\text{NH}_3$  partial current density on the simple Ni foam is among the highest performances by far in the field (Fig. 2b and Table S1, ESI†), which is roughly double that on the Co-NAs<sup>14</sup> ( $2.23 \text{ A cm}^{-2}$  at room temperature) and quadruple that on the Ru-CuNWs<sup>15</sup> ( $0.965 \text{ A cm}^{-2}$  at room temperature). At lower current densities, the  $\text{NO}_3^-$  conversion can be improved to 94.5–96.5% at 100–500  $\text{mA cm}^{-2}$ , while maintaining a high level of FE for  $\text{NH}_3$  (84.0%–92.2%) (Fig. S4b, ESI†). Furthermore, the MFAEL system can function efficiently at temperatures up to 200 °C without considerable decrease in the FE towards  $\text{NH}_3$  or  $\text{NO}_3^-$  conversion (Fig. 2d and Fig. S5, ESI†). Notably, raising the initial  $\text{NO}_3^-$  concentration can further enhance the FE towards  $\text{NH}_3$  to 99.5% at 500  $\text{mA cm}^{-2}$ , while the  $\text{NO}_3^-$  conversion remained high (98.8%) (Fig. 2e).

A series of control experiments performed in this study (Fig. S6, ESI†) confirms that the observed  $\text{NH}_3$  production is indeed from the electro-reduction of  $\text{NO}_3^-$ , without considerable interference from the contamination of other Nr (other than  $\text{NO}_3^-$ ), non-faradaic reactions between the electrode and  $\text{NO}_3^-$ , or the reaction between  $\text{NO}_3^-$  and  $\text{H}_2$ . The accuracy of  $\text{NH}_3$  quantification was cross-verified by comparing the results obtained from indophenol colorimetry (adopted method in this work) with <sup>1</sup>H NMR and ion chromatography, and the difference in their results was <5% (Fig. S7, ESI†).

Online gas chromatography (GC) also confirmed that the HER is largely suppressed with a very low level of FE (*e.g.*, an average FE of 5.35% at 250  $\text{mA cm}^{-2}$ ), and  $\text{N}_2$  generation was not detected during the entire course of electrolysis (Fig. 2c and S8, ESI†). These results are in concert with the close-to-unity balance of N element (considering  $\text{NO}_3^-$ ,  $\text{NO}_2^-$ , and  $\text{NH}_3$ ) for all measurements (Table S2, ESI†), showing that  $\text{NH}_3$  is the exclusive favorable product of NO3RR in the NaOH/KOH/ $\text{H}_2\text{O}$  electrolyte. Note that the observed FE towards  $\text{NO}_2^-$  was lower than 6% for all measurements, indicating the facile sequential reduction of N–O bonds towards the fully hydrogenated product  $\text{NH}_3$ .

Interestingly, replacing the carrier gas (high-purity  $\text{N}_2$ ) with air or high-purity  $\text{O}_2$  does not induce any considerable change in the cell performance (Fig. S9, ESI†), demonstrating the



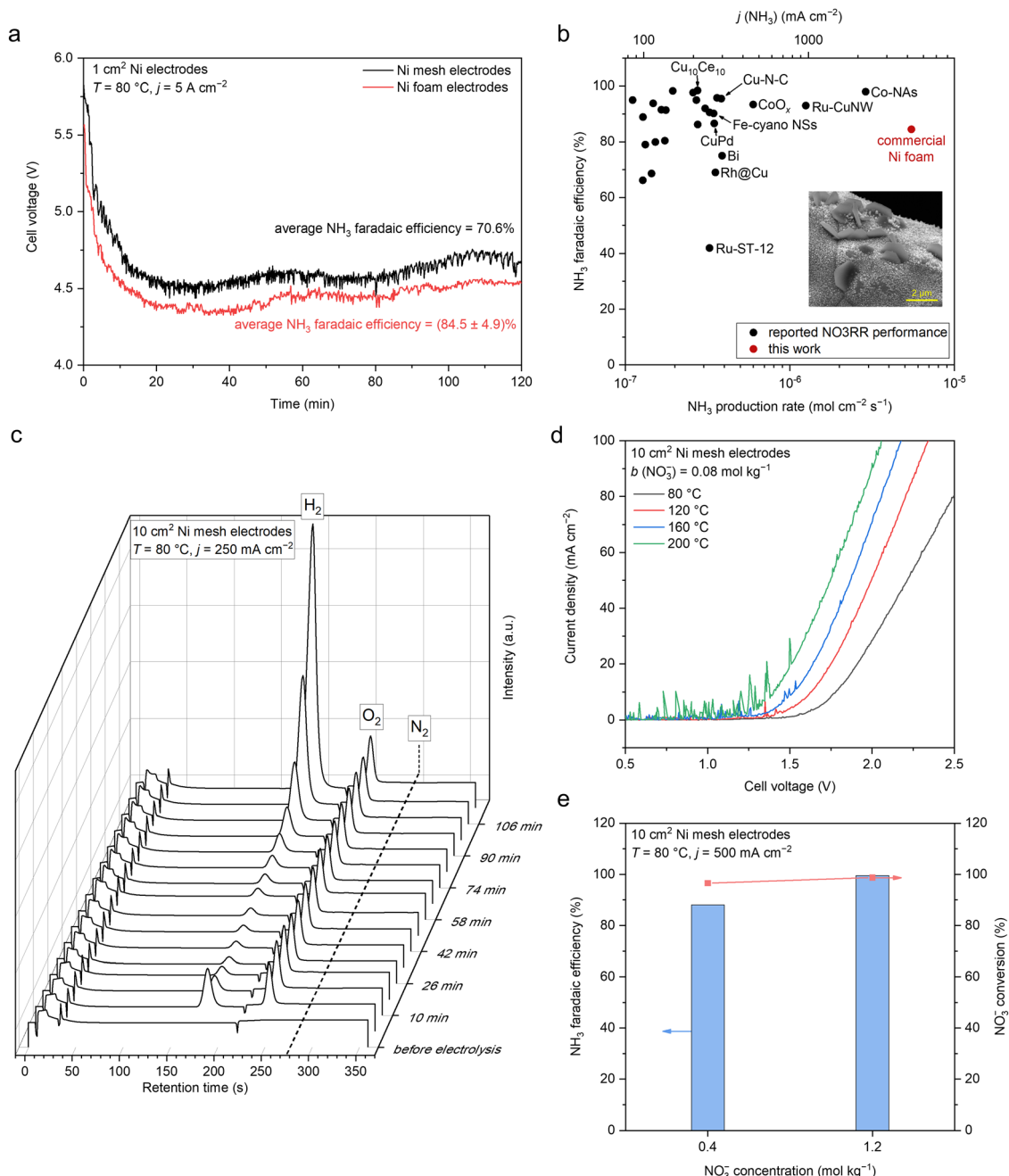


**Fig. 2** Electrochemical NH<sub>3</sub> production by NO<sub>3</sub>RR in the NaOH/KOH/H<sub>2</sub>O electrolyte in MFAEL. (a) Cell voltage profiles of the 2-hour NO<sub>3</sub>RR test at 5 A cm<sup>-2</sup> using two identical Ni mesh or Ni foam electrodes (1 cm<sup>2</sup> geometric area). (b) Comparison of the NO<sub>3</sub>RR performance in this work with reported state-of-the-art performances. Data are summarized in Table S1 (ESI<sup>†</sup>). The inset shows the SEM image of the post-electrolysis Ni foam cathode. (c) Profile of online GC (with 99.999% Ar as the carrier gas) graphs during the 2-hour NO<sub>3</sub>RR test in MFAEL at 250 mA cm<sup>-2</sup>. The retention time was 187 s for H<sub>2</sub>, 248 s for O<sub>2</sub>, and 278 s for N<sub>2</sub>. Only a trace level of N<sub>2</sub> (~400 ppmv) was detected throughout the electrolysis, corresponding to <1% FE towards N<sub>2</sub>. Note that this value is close to the background concentration of N<sub>2</sub>, confirming that NO<sub>3</sub>RR in the NaOH/KOH/H<sub>2</sub>O electrolyte strongly favors the production of NH<sub>3</sub>, and the N–N coupling pathway is inhibited. (d) LSV curves in the NaOH/KOH/H<sub>2</sub>O electrolyte with 0.08 mol kg<sup>-1</sup> of added KNO<sub>3</sub> at different temperatures. The scan rate was 100 mV s<sup>-1</sup>. (e) Comparison of NO<sub>3</sub>RR performance with different initial NO<sub>3</sub><sup>-</sup> concentrations in the electrolyte. Note that the applied charge was equal to the theoretical charge required for the full conversion of the added KNO<sub>3</sub> into NH<sub>3</sub>; therefore at j = 500 mA cm<sup>-2</sup>, the electrolysis duration was 2 and 6 hours for the left and right columns, respectively.

robustness of the MFAEL system, as inexpensive air can be used to realize efficient product separation without interference from the O<sub>2</sub> content. Separating the catholyte and anolyte with a porous PTFE mesh resulted in a similarly high FE (86.7%,

Fig. S10, ESI<sup>†</sup>), which strongly suggests that the co-generated H<sub>2</sub> and O<sub>2</sub> have minimal impact on the performance of the NO<sub>3</sub>RR.

High alkalinity of NaOH/KOH/H<sub>2</sub>O electrolyte is a critical prerequisite for the high-efficiency NO<sub>3</sub><sup>-</sup>-to-NH<sub>3</sub> conversion in



MFAEL. 1:1 molar NaOH/KOH was chosen to constitute the ternary NaOH/KOH/H<sub>2</sub>O electrolyte for this study due to the optimal performance and the maximum window for tuning water content, compared to the binary NaOH/H<sub>2</sub>O or KOH/H<sub>2</sub>O compositions (Fig. S11a, ESI†).<sup>23</sup> Increasing the water content of the electrolyte from 40 wt% to 91 and 99 wt% (40, 91, and 99 wt% of water content corresponds to 15, 2, and 0.2 M of OH<sup>-</sup> concentration, respectively) leads to a significant decrease in the FE towards NH<sub>3</sub> and the NO<sub>3</sub><sup>-</sup> conversion (Fig. S11b, ESI†). In addition, higher alkalinity facilitates the evolution of produced NH<sub>3</sub> from the MFAEL reactor, as observed from the distribution of NH<sub>3</sub> after electrolysis (Fig. S11c, ESI†). These tendencies agree with the thermodynamic calculation results in Fig. S2 (ESI†). The type of chosen alkali for the electrolyte has modest effect on the NO<sub>3</sub>RR performance at high alkalinity (15 M OH<sup>-</sup>, Fig. S11a, ESI†); with 2 M OH<sup>-</sup>, an apparent cationic effect was observed, and FE towards NH<sub>3</sub> shows the discernable trend of Li<sup>+</sup> < Na<sup>+</sup> < K<sup>+</sup> (Fig. S11d, ESI†).

Notably, the re-deposition of partially oxidized nickel species on the cathode was observed during electrolysis, which extends the electrochemical surface area contributing to the high-performance NO<sub>3</sub><sup>-</sup>-to-NH<sub>3</sub> conversion. No substantial change was found on the anode in the post-electrolysis characterization by scanning electron microscopy (SEM), while the formation of nanoparticles of ~100 nm and larger hexagonal flakes of 1–2.5 μm were found on the cathode (Fig. 2b and Fig. S12, ESI†), in accordance with the observed darkening of the cathode subject to electrolysis (Fig. S13, ESI†).

The energy-dispersive X-ray spectroscopy (EDS) analysis reveals the Ni/O atomic ratio of 3.66 and 0.72 on the nanoparticles, respectively; and an overall increase in oxygen content from 1.2 at% before electrolysis to 24.3 at% afterwards (Fig. S14–S16, ESI†). The surface of the post-electrolysis cathode consists of a layer of Ni(OH)<sub>2</sub>, as suggested by XPS and Raman spectra (Fig. S17, ESI†). These deposits increased the roughness factor (RF) of the Ni cathode by 1.11 and 1.69 times for Ni mesh and Ni foam, respectively (Fig. S18, ESI†), which should be a contributor to the enhancement of the NO<sub>3</sub>RR activity.

The formation of those cathodic deposits should come from the migration of Ni from the anode to the cathode during electrolysis (namely, re-deposition): anodic Ni is initially oxidized to Ni(OH)<sub>2</sub>/NiOOH which is an active catalyst for the oxygen evolution reaction (OER),<sup>24</sup> followed by its partial dissolution in a strongly alkaline electrolyte in the forms of Ni(OH)<sub>3</sub><sup>-</sup> or Ni(OH)<sub>4</sub><sup>2-</sup>;<sup>25</sup> subsequently, these soluble Ni(II) species are re-deposited onto the cathode. When a Cu mesh was used as the cathode while keeping the Ni mesh as the anode, similar deposits were observed (Fig. S19 and S20, ESI†); however, when a graphite rod was used as the anode while using Ni foam as the cathode, no deposit was observed after electrolysis (Fig. S21, ESI†). Clearly, the two experiments verified that the origin of those deposits is the Ni anode. As such, the re-deposition of Ni-species in this work should be distinguished from the “cathodic corrosion” reported by Koper *et al.*<sup>26</sup> Also, the re-deposition process is possibly associated with the higher cell voltage and lower FE towards NH<sub>3</sub> at the initial period of electrolysis (as shown in Fig. 2a and c).

It should be noted that such a re-deposition occurs only within the near-surface region of the electrodes while the bulk composition of the electrodes remains largely unchanged, as evidenced by the X-ray diffraction (XRD) (Fig. S17a, ESI†). This is also consistent with the very minor change in mass of the Ni electrodes (<1 mg) operated at 5 A for 2 hours. In real applications, the longevity of both Ni electrodes can be maintained by periodically reversing the current flow.

### Production of pure NH<sub>3</sub>-based chemicals from a scale-up MFAEL

Thanks to the high activity and operational robustness of the MFAEL, we increased the reaction capacity from 100 mL to 2.5 L under industrial-level current density (Fig. S23, ESI†). Two 100 cm<sup>2</sup> Ni mesh electrodes were folded and immersed in the electrolyte, and a constant current of 25 A was applied (*i.e.*, 250 mA cm<sup>-2</sup>). With the scaled-up system, NO<sub>3</sub>RR was carried out for 24 hours, resulting in an average FE of 70.4% towards NH<sub>3</sub> and a steady-state cell voltage of 2.7 V (Fig. 3a). As a result, a very high NH<sub>3</sub> production rate of 82.1 mmol h<sup>-1</sup> was achieved in this scaled-up MFAEL reactor.

The produced NH<sub>3</sub> from the MFAEL can be managed in different forms: NH<sub>4</sub><sup>+</sup> salts (such as sulfate), aqueous NH<sub>3</sub> solutions, and a solid NH<sub>4</sub>HCO<sub>3</sub> product (Fig. 1c). When an acidic absorbing solution (*e.g.*, H<sub>2</sub>SO<sub>4</sub> solution) is used as for most measurements in this work, NH<sub>4</sub><sup>+</sup> salts are the final products in solution. The collection efficiency is almost 100% under varying conditions, as evidenced by the close-to-unity N balance for all tests (Table S2, ESI†).

Alternatively, when water (5 °C) is used for NH<sub>3</sub> absorption, despite a slightly lower collection efficiency (95.6%) (Fig. S23a, ESI†), a highly-concentrated NH<sub>3</sub> solution (4.13 M, or around 7 wt%) was obtained after the 24 hour electrolysis from the scaled-up MFAEL. The MFAEL-derived NH<sub>3</sub> solution (with added 1.25 M KOH) was directly supplied as the anode fuel for an anion-exchange membrane fuel cell (Fig. 3b and Fig. S24, ESI†), outputting a peak power density of 33.7 mW cm<sup>-2</sup> at 80 °C, which is a reasonable performance among the reported values of direct NH<sub>3</sub> fuel cells using commercial catalysts, membranes, and ionomers.<sup>27</sup> Notably, the *I*-*V* curve and power density profile show no significant difference between the fuel cells fed with MFAEL-derived NH<sub>3</sub> solution and that fed with a commercial NH<sub>3</sub> solution of the same concentration, suggesting the high purity of the MFAEL-derived NH<sub>3</sub> solution.

In another case, the NH<sub>3</sub>-containing outlet gas from MFAEL was absorbed by a CO<sub>2</sub>-bubbling water solution at 5 °C. Owing to the acidity of CO<sub>2</sub>, NH<sub>3</sub> collection efficiency as high as 99.9% was achieved (Fig. S23a, ESI†). Co-absorbing NH<sub>3</sub> and CO<sub>2</sub> in water produces NH<sub>4</sub>HCO<sub>3</sub> with the simultaneous collection of NH<sub>3</sub> and the capture of waste CO<sub>2</sub>. Due to the limited solubility of NH<sub>4</sub>HCO<sub>3</sub> (around 14.3 g in 100 mL water at 5 °C), its precipitation is well controlled by altering the volume and temperature of the absorbing solution: after 24 hour electrolysis in the scaled-up MFAEL, the precipitate in the absorbing solution (5 °C) was collected by vacuum filtration, ethanol washing, and drying under ambient conditions. 74.2 g of solid



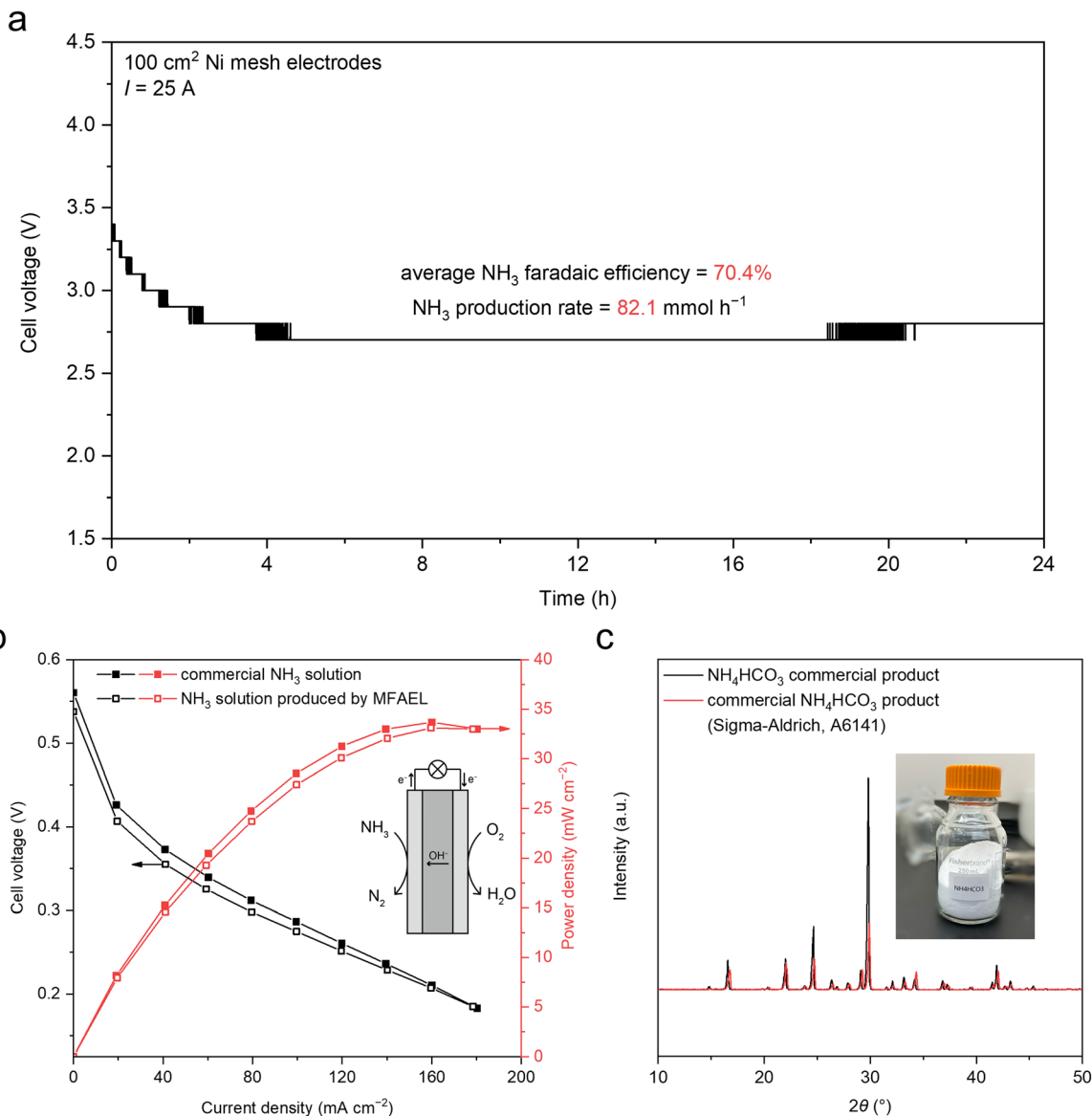


**Fig. 3** Producing pure  $\text{NH}_3$ -based chemicals in a scaled-up MFAEL system. (a) Cell voltage profile for the scaled-up MFAEL system in a 24-hour  $\text{NO}_3\text{RR}$  test at 25 A. Note that the steps in the voltage profile are due to the minimum resolution of our DC power supply (0.1 V) at the large current rating (30 A). (b) Polarization and power density curves for the fuel cells with MFAEL-derived  $\text{NH}_3$  solution and commercial  $\text{NH}_3$  solution (with the same concentration) as the anode fuel. The fuel cell was operated at  $80^\circ\text{C}$ , and 1.25 M KOH was added to the  $\text{NH}_3$  solutions. (c) XRD patterns of the MFAEL-derived  $\text{NH}_4\text{HCO}_3$  solid and a commercial  $\text{NH}_4\text{HCO}_3$  product. The inset photo shows the collected  $\text{NH}_4\text{HCO}_3$  product (74.2 g) from 24 hour electrolysis in a scaled-up MFAEL.

$\text{NH}_4\text{HCO}_3$  product was obtained and its high purity was confirmed by XRD (Fig. 3c and Fig. S23, ESI†). One further use of such  $\text{NH}_4\text{HCO}_3$  involves a bicarbonate electrolyzer with a bipolar membrane, in which  $\text{CO}_2$  is generated *in situ* and reduced to formate, CO, or other value-added products.<sup>28,29</sup>

#### Electrodialysis for energy-efficient concentration of $\text{NO}_3^-$

$\text{NO}_3^-$  is one of the most abundant and widespread forms of N in nature, and therefore recovering  $\text{NO}_3^-$  from dilute waste streams (on levels of tens or hundreds of ppm  $\text{NO}_3^-$ -N<sup>12</sup>) and concentrating it into sufficient concentrations (such as 1 or 2 M) is an indispensable step of the  $\text{NO}_3^-$  treatment by

high-rate  $\text{NH}_3$ -producing electrolysis. Compared with reverse osmosis (RO), ion exchange (IX), and other  $\text{NO}_3^-$ -recovering technologies, electrodialysis (ED) is particularly suitable for low- to medium-concentration  $\text{NO}_3^-$  feedstocks, because of its lower energy consumption (*cf.* RO) and much smaller chemical consumption (*cf.* IX). For typical industrial ED systems, a few hundred electrodialysis pairs are assembled between one set of electrodialysis electrodes, and a single electrodialysis pair is often constructed by the configuration of “CEM | diluate | AEM | concentrate”, where CEM and AEM stand for cation-exchange membrane and anion-exchange membrane, respectively; and diluate and concentrate stand for the  $\text{NO}_3^-$ -giving feedstock



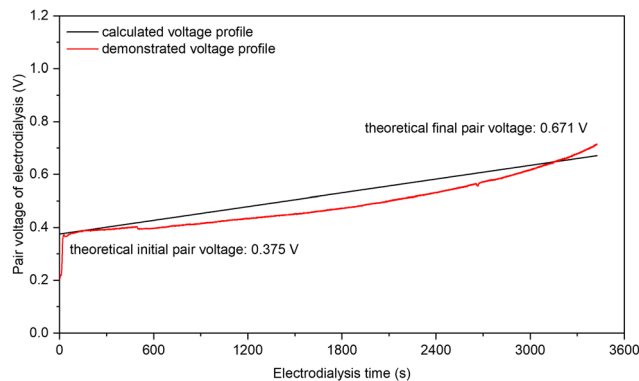


Fig. 4 The voltage profiles of one electrodiagnosis pair along with electrodiagnosis time for  $\text{NO}_3^-$  concentration. A single electrodiagnosis pair is constructed by the configuration of “CEM | diluate | AEM | concentrate” in which the CEM and the AEM are FKA-PK-130 and FAA-PK-130, respectively, both from Fuma-Tech; and the diluate and the concentrate are 7.14 mM  $\text{KNO}_3$  (100 ppm  $\text{NO}_3^-$ -N) and 2 M  $\text{KNO}_3$  (28 000 ppm  $\text{NO}_3^-$ -N), respectively. The key experimental conditions include: 5  $\text{cm}^2$  as the effective pair area, 1  $\text{mA cm}^{-2}$  as the electrodiagnosis current density, 10  $\text{cm s}^{-1}$  as the nominal fluid velocity for all channels (60  $\text{mL min}^{-1}$ ), 0.5 mm as the distance between CEM and AEM in the electrodiagnosis pair, and 75% as the designed  $\text{NO}_3^-$  removal (3444 seconds). Note that the applied current density for ED is subject to the threshold set by the “limiting current density” calculated by the Rosenberg and Tirrell equation,<sup>41</sup> and the obtained limiting current density is 4.62 and 1.19  $\text{mA cm}^{-2}$  at the initial (7.14 mM) and the final diluate concentration (1.79 mM), respectively, under our experimental conditions.

solution and the  $\text{NO}_3^-$ -receiving product solution, respectively. As such, the “pair voltage” arising from a single electrodiagnosis pair largely controls the energy consumption of ED, in addition to the pumping-caused energy consumption.

We have experimentally verified that the low pair voltage for concentrating  $\text{NO}_3^-$  by ED is achievable and predictable with a small intermembrane distance of 0.5 mm and a sufficient fluid velocity of 10  $\text{cm s}^{-1}$  (Fig. S25, ESI<sup>†</sup>). Fig. 4 shows the pair voltage profile of our ED experiment of concentrating 7.14 mM (100 ppm  $\text{NO}_3^-$ -N) into 2 M  $\text{NO}_3^-$  (28 000 ppm  $\text{NO}_3^-$ -N) with 75% of the designed  $\text{NO}_3^-$  recovery at an appropriate ED current density of 1  $\text{mA cm}^{-2}$ . The observed initial and final pair voltage was 0.39 and 0.63 V, respectively, both of which are highly consistent with the theoretical predictions (0.376 and 0.671 V, respectively) by considering both the Donnan potential rise (from both cation and anion) and the ohmic potential rise (from two membranes and two solutions). The observed coulombic efficiency of  $\text{NO}_3^-$  concentration was 96%. A consistent pair voltage profile with the predicted one was also observed at 2  $\text{mA cm}^{-2}$  (Fig. S26, ESI<sup>†</sup>). Our experimental verification on low pair voltage and high coulombic efficiency is the first result in the  $\text{NO}_3^-$  concentrating with low concentrations by electrodiagnosis to our best knowledge. Considering the  $\text{NO}_3^-$  concentration in the real-world waste streams, the  $\text{NO}_3^-$  recovery is deemed feasible.

### Techno-economic analysis of upcycling $\text{NO}_3^-$ -N from dilute waste streams

To better understand the economic viability of concentrating  $\text{NO}_3^-$  by ED and its subsequent conversion to  $\text{NH}_3$  in MFAEL,

a model of techno-economic analysis (TEA) was established in this study.

**Electrodiagnosis for concentrating  $\text{NO}_3^-$ .** For ED, the operational expense (OPEX) was solely considered from energy consumption that has two major contributing sources: electrodiagnosis (pair voltage and current) and pumping (pair pressure drop and flow rate). Then, the “levelized total cost” (LTC) was obtained by summing OPEX and the levelized capital cost (LCC), depending on detailed operational conditions and concentrating requirements (Fig. S27 and S28, ESI<sup>†</sup>). In a typical case with 7.14 mM (100 ppm  $\text{NO}_3^-$ -N) of the initial diluate concentration, 2 M (28 000 ppm  $\text{NO}_3^-$ -N) of the concentrate concentration, 80% of  $\text{NO}_3^-$  recovery, 4  $\text{cm s}^{-1}$  of nominal fluid velocity, 0.5 mm of pair distance, and \$0.07  $\text{kW h}^{-1}$  of electricity price, the obtained LTC is merely \$5.75 per  $\text{kmol-NO}_3^-$ .

Fig. 5a presents a contour map of LTC with respect to the diluate concentration and  $\text{NO}_3^-$  recovery, both of which are related to the workload and requirement of  $\text{NO}_3^-$  feedstock. Clearly, the LTC sharply decreases with increasing diluate concentration and mildly increases with raising  $\text{NO}_3^-$  recovery. The concentration of initial diluate is the most influential parameter, and its impacts on OPEX and LCC are presented in Fig. 5b. The LTC is dominated by OPEX and LCC for the initial diluate concentration ranges of <100 and >300 ppm  $\text{NO}_3^-$ -N, respectively. This trend is essentially driven by the exponentially-growing energy consumption from both ED operation and fluid pumping when lowering the  $\text{NO}_3^-$  concentration in the diluate solution. By contrast, the impact of electricity price is simply linear to OPEX (Fig. S29, ESI<sup>†</sup>).

**NO<sub>3</sub>RR for  $\text{NH}_3$  production.** The TEA of NO<sub>3</sub>RR for  $\text{NH}_3$  production in MFAEL was also performed (Fig. S30 and S31, ESI<sup>†</sup>). Capital cost analysis was performed based on a customized medium-size MFAEL reactor with 100 L electrolyte capacity and a total electrode area of 3.36  $\text{m}^2$ . The cost of all identified materials and ancillary/auxiliary parts/components was estimated to be \$1164 per system. Next, considering all unidentified parts (10%) and all other associated costs,<sup>30</sup> the total capital cost of this electrolyzer system was projected to be \$3121 per system. Based on the total capital cost (\$3121 per system) and the standard capital recovery method, the LCC for  $\text{NO}_3^-$  electrolysis was calculated to be \$0.97 per  $\text{kmol-NH}_3$ , on the following assumptions: 20 years of service time, 19% as the cost ratio of maintenance to the system, 3% of annual discount rate,<sup>31</sup> 83.3% of capacity factor, and 90% of faradaic efficiency. Such a low level of LCC for NO<sub>3</sub>RR is due greatly to the inexpensive materials (nickel mesh, stainless steel, and PTFE) used to construct the MFAEL system.

The OPEX of NO<sub>3</sub>RR was solely calculated from energy consumption at a certain electricity price. In addition to the electrolysis (cell voltage and current), the energy consumptions from both mixing and heating are considered.

Fig. S32 (ESI<sup>†</sup>) shows the strong relationship between the energy consumption and the cell voltage of NO<sub>3</sub>RR, largely because the mixing consumes significantly less energy than the electrolysis (e.g., 0.17 vs. 45.03  $\text{kW h}$  per  $\text{kmol-NH}_3$  under 2.7 V of cell voltage at 250  $\text{mA cm}^{-2}$ ). The contour map for the LTC of



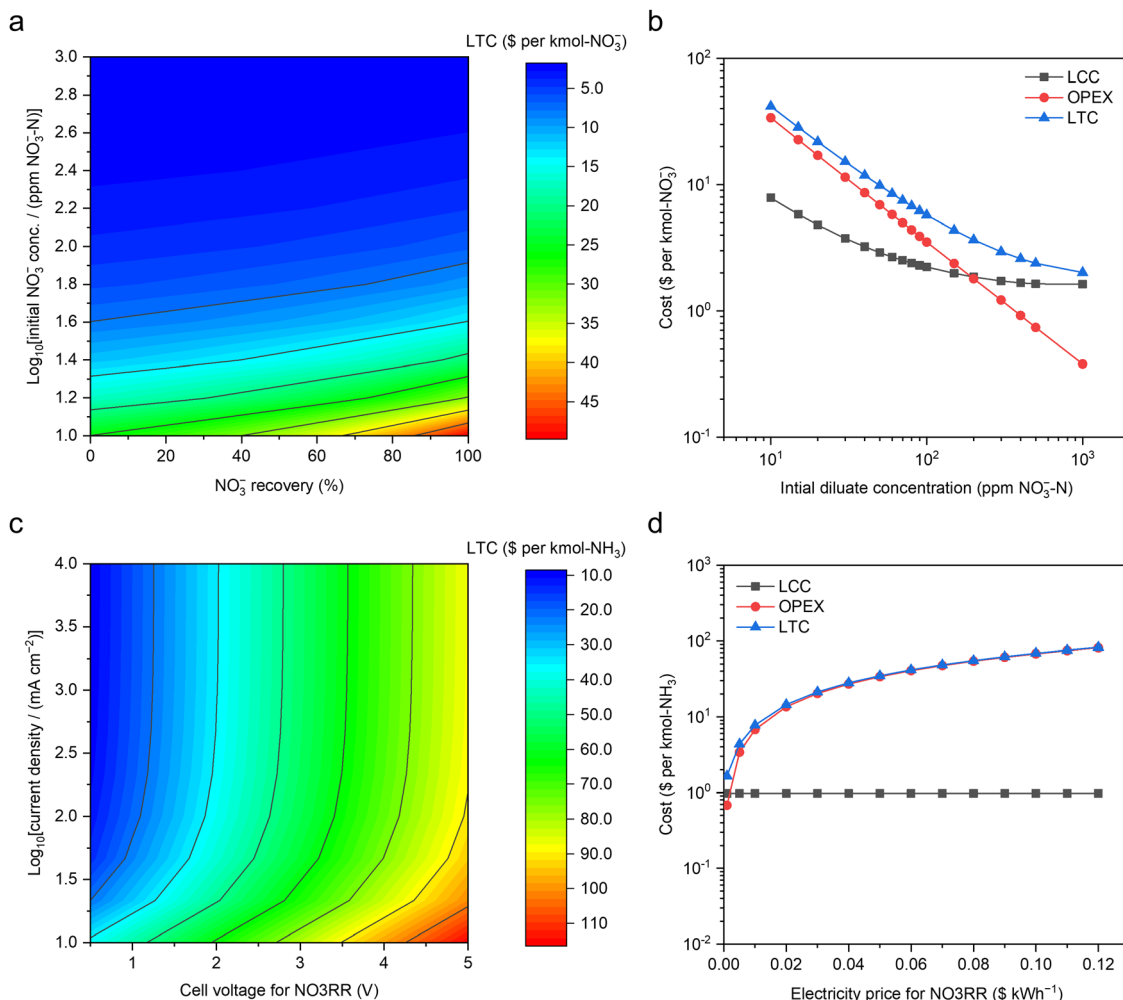


**Fig. 5** Techno-economic analysis of upcycling  $\text{NO}_3^-$ -N from dilute waste streams. (a) The contour map for the LTC of  $\text{NO}_3^-$  concentration by electrodiolysis with respect to the initial  $\text{NO}_3^-$  concentration in the diluate and the designed  $\text{NO}_3^-$  recovery from the diluate ( $\$0.07 \text{ kW h}^{-1}$  of electricity cost). (b) LTC, OPEX, and LCC along with the initial diluate concentration ( $\$0.07 \text{ kW h}^{-1}$  of electricity price and 80% of designed  $\text{NO}_3^-$  recovery). Based on a typical medium-size commercial electrodiolysis system (40 cm  $\times$  160 cm for each electrodiolysis pair, and 250 electrodiolysis pairs in total), the LCC was calculated via the standard capital recovery method, assuming 40 years of service time,<sup>42</sup> 19% as the cost ratio of maintenance to the system, 3% of annual discount rate,<sup>31</sup> 83.3% of capacity factor, and 90% of coulombic efficiency. (c) The contour map for the LTC of  $\text{NH}_3$  production by NO3RR in MFAEL with respect to the electrolytic current density and cell voltage ( $\$0.07 \text{ kW h}^{-1}$  of electricity price). (d) The impact of electricity price on the LTC and OPEX of the NO3RR (2.7 V of cell voltage and  $250 \text{ mA cm}^{-2}$  of current density). Capital cost analysis was performed based on a customized medium-size MFAEL reactor with 100 L electrolyte capacity with the total electrode area of  $3.36 \text{ m}^2$ . The cost of all identified materials and ancillary/auxiliary parts/components was estimated to be  $\$1164$  per system. Considering all unidentified parts (10%) and all other associated costs,<sup>30</sup> the total capital cost of this electrolyzer system was projected to be  $\$3121$  per system. Other assumptions and methodologies are discussed in the ESI†.

NO3RR in  $\$$  per  $\text{kmol-NH}_3$  with respect to the electrolytic current density and cell voltage was presented in Fig. 5c, assuming  $\$0.97 \text{ kmol-NH}_3$  as the LCC and  $\$0.07 \text{ kW h}^{-1}$  as the electricity price. Consistent with Fig. S32 (ESI†), cell voltage is a dominant parameter controlling the LTC for NO3RR. Increasing the current density leads to a decrease in the LTC (Fig. S33, ESI†), but its impact is most pronounced below  $50 \text{ mA cm}^{-2}$ ; at higher current densities, the LTC is overwhelmingly dominated by the OPEX, suggesting that future improvement should be primarily focused on lowering the cell voltage of the MFAEL. It should be pointed out that the observed trend with respect to current density is greatly attributed to the very low level of LCC, thanks to the inexpensive and durable materials used in the system (such as

nickel and stainless steel). When expensive or non-durable catalytic materials are used, the LTC could be comparable to the OPEX. Owing to the major contribution of the energy cost to the LTC, future decrease in the electricity price will also be greatly beneficial to lowering the LTC (Fig. 5d). Though higher current density does not substantially lower the LTC of the MFAEL system, it does offer a level of system flexibility of operating at a reduced capacity factor to benefit from the lower-priced or even free electricity from excessive renewable generation. The advantage of utilizing cheap/free electricity may significantly reduce the LTC, in light of the heavy energy consumption.

On the assumptions above, the LTC of NO3RR in MFAEL under our typical operating conditions (2.7 V and  $250 \text{ mA cm}^{-2}$ )



turns out to be \$48.42 per kmol-NH<sub>3</sub>. Note that the OPEX related to heating is merely \$2.25 per kmol-NH<sub>3</sub> (Fig. S31, ESI†), which is only 4.6% of the LTC of NO<sub>3</sub>RR. Considering the low LTC for concentrating NO<sub>3</sub><sup>-</sup> (\$5.75 per kmol-NO<sub>3</sub><sup>-</sup>) by ED, our newly-proposed upcycling strategy not only offers a lower cost (*i.e.*, \$54.57) compared to the current cost of N removal in wastewater treatment plants (around \$65 per kmol-N<sup>32</sup>), but also leaves a competitive profit margin with the market price of NH<sub>3</sub> (\$9.35 per kmol).

### A convergent Nr-to-NH<sub>3</sub> process enabled by MFAEL

Thus far, the OER has been the anodic reaction in the investigated systems, which does not produce value-added products itself. Alternatively, a paired electrolysis system can be constructed by combining the reduction of NO<sub>3</sub><sup>-</sup> (on cathode) and oxidation of C–N bonds in organic Nr compounds (on anode) in one electrolytic cell (Fig. 6a). Organic Nr compounds (such as amino acids and proteins) represent a large portion of the

global inventory of Nr (Fig. 1b), but their chemical conversion remains challenging owing to the high stability of C–N bonds.<sup>33</sup> In such a paired system, organic Nr serves as an additional source of N for NH<sub>3</sub> production and provides electrons for NO<sub>3</sub><sup>-</sup> reduction. Meanwhile, the anode product is switched from low-value O<sub>2</sub> (through OER) to value-added oxidized organic compounds such as carboxylic acids with the simultaneous release of NH<sub>3</sub>, increasing economic feasibility.

To examine the NH<sub>3</sub> formation from organic Nr in NaOH/KOH/H<sub>2</sub>O, we first screened a series of N-containing compounds with representative chemical environments of N element (12 organic Nr compounds and 3 inorganic Nr compounds) at 200 °C with an applied current density of 25 mA cm<sup>-2</sup> (Fig. 6b and Table S3, ESI†). Note that most organic Nr compounds we examined in this work are amino acids (listed in Table S3, ESI†), which are common and major forms of organic N in the ecosystems.<sup>34</sup> Interestingly, except for EDTA (ethylenediaminetetraacetic acid) and TMG (trimethyl glycine), N from all other

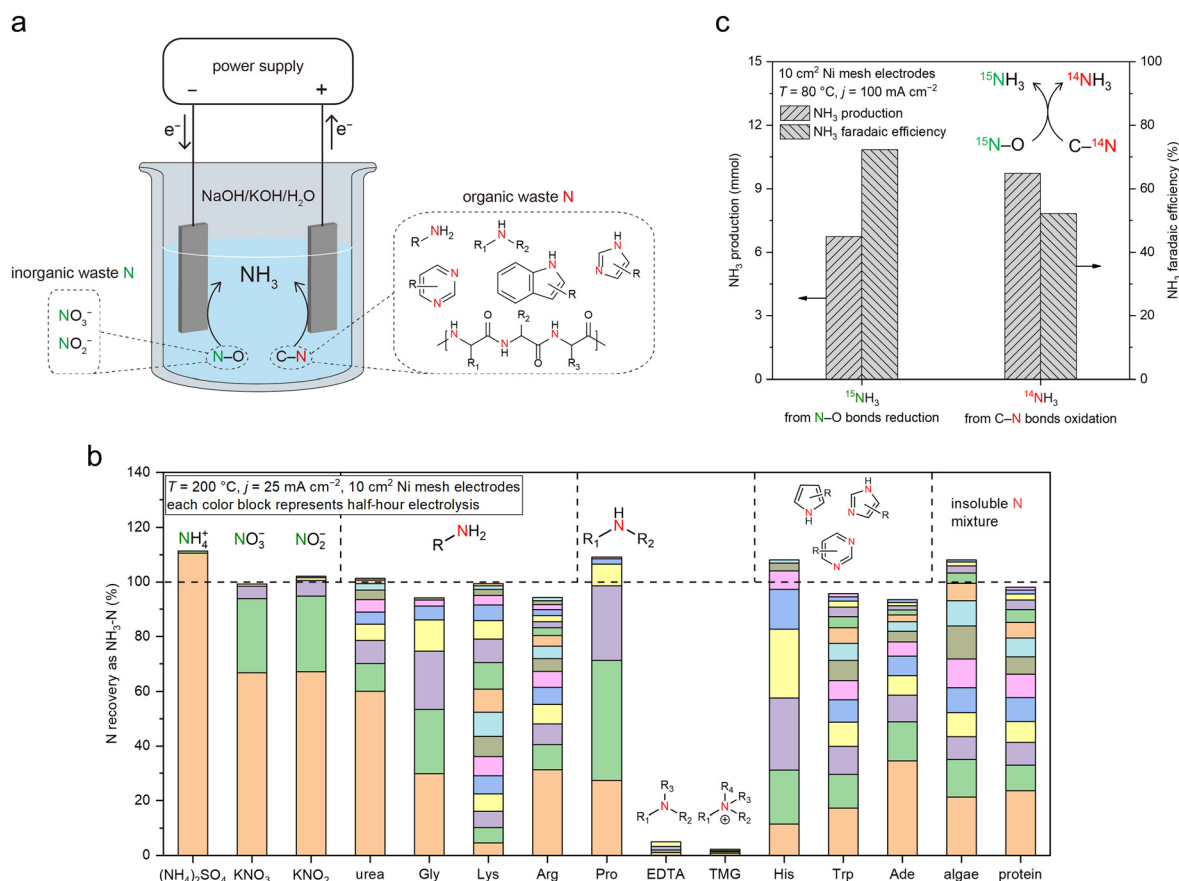
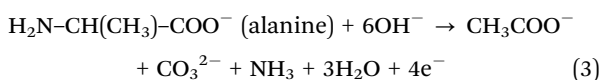
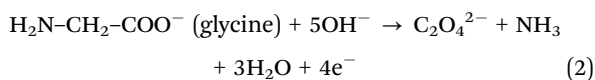


**Fig. 6** A convergent Nr-to-NH<sub>3</sub> process enabled by MFAEL. (a) Illustration of the proposed concept, in which the waste materials containing N–O bonds (inorganic wastes) and C–N bonds (organic wastes) are simultaneously converted to NH<sub>3</sub> in MFAEL as the sole N-containing product. (b) Screening test results for different forms of Nr. Electrolysis was carried out at 25 mA cm<sup>-2</sup> and 200 °C with 0.2 mmol of added N for each chemical, and NH<sub>3</sub> was collected every half hour until no significant increase in its production was detected. The y-axis (NH<sub>3</sub>-N recovery) corresponds to the ratio of the produced NH<sub>3</sub>-N to the initially added Nr-N. Each color block represents the NH<sub>3</sub> production from a half-hour period. The representative chemical structures of the Nr compounds are labeled on the top of the columns. Detailed reactant abbreviations, structures, and test results are summarized in Table S3 (ESI†). (c) Production of and FE towards <sup>14</sup>NH<sub>3</sub> and <sup>15</sup>NH<sub>3</sub> during the paired electrolysis in MFAEL containing both <sup>15</sup>N–O and C–<sup>14</sup>N bonds. K<sup>15</sup>NO<sub>3</sub> (9.3 mmol) and alanine (18.7 mmol) were chosen as the model chemicals containing <sup>15</sup>N–O and C–<sup>14</sup>N bonds, respectively. The produced <sup>14</sup>NH<sub>3</sub> and <sup>15</sup>NH<sub>3</sub> were quantified by <sup>1</sup>H NMR.



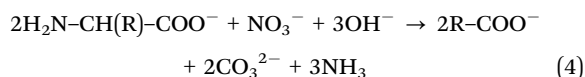
N-containing compounds (10 in organic Nr and 3 in inorganic Nr) examined in this work was completely converted to NH<sub>3</sub> in its final form within a few hours of electrolysis. Compared to inorganic Nr (with N–O bonds), organic Nr compounds require longer reaction time for full conversion, because of the higher stability of C–N bonds.<sup>35</sup> N atoms connected with longer carbon chains, conjugated structures, or more than two adjacent C atoms appear to be less reactive, though in most cases they can ultimately be converted to NH<sub>3</sub>. The high Nr conversion and high NH<sub>3</sub> selectivity enable a convergent pathway from various forms of Nr towards NH<sub>3</sub> as the sole N-containing product.

We then investigated the products after the cleavage of C–N bonds in NaOH/KOH/H<sub>2</sub>O (Fig. S34, ESI†). Glycine and alanine were chosen as the reactants due to their structural simplicity, and electrolysis was performed at 80 °C. To track the carbon-containing products, <sup>13</sup>C-labeled chemicals were used as the reactants, and the products were analyzed by <sup>13</sup>C nuclear magnetic resonance (NMR) spectroscopy. The results show that the oxidations of both organic Nr compounds are 4-electron-transfer processes, in which the C–N bond scission is accompanied by the oxidation of the C element and the release of NH<sub>3</sub>. Upon the cleavage of the C–N bond, the identified product for glycine oxidation was oxalate; while for alanine, a subsequent decarboxylation occurs, giving rise to acetate and carbonate (eqn (2) and (3) below):



Similar results should be expected for Nr in more complex structures, demonstrating that MFAEL is capable of converting organic N-containing wastes into value-added carboxylic acid products, while largely retaining the skeleton of the original molecules. Additional experimental results (detailed in Fig. S35 and S36, ESI†) confirmed that both applied electricity and high alkalinity are indispensable conditions for the reaction to proceed efficiently in MFAEL. In the presence of organic Nr, production of O<sub>2</sub> from OER is apparently suppressed as confirmed by online GC (Fig. S37, ESI†). Interestingly, none of the volatile carbon-containing products (CO, CH<sub>4</sub>, CO<sub>2</sub>, C<sub>2</sub>H<sub>2</sub>, C<sub>2</sub>H<sub>4</sub>, and C<sub>2</sub>H<sub>6</sub>) was detected by online GC during the conversion of organic Nr (Fig. S38, ESI†), indicating that carbon is retained in the electrolyte.

Knowing that NH<sub>3</sub> can be produced *via* the oxidation-assisted cleavage of C–N bonds, we paired the reduction of N–O bonds with the oxidation of C–N bonds, aiming to generate NH<sub>3</sub> from both sources (Fig. 6c and Fig. S39, ESI†). For this purpose, KNO<sub>3</sub> and alanine were added into MFAEL as model reactants containing N–O and C–N bonds:



Notably, to determine the respective contribution of NH<sub>3</sub> production from each source, the N–O reactant was isotopically

labeled using K<sup>15</sup>NO<sub>3</sub>, and the NH<sub>3</sub> product was analyzed by <sup>1</sup>H NMR to differentiate <sup>14</sup>NH<sub>3</sub> and <sup>15</sup>NH<sub>3</sub>. With this configuration operated at 100 mA cm<sup>-2</sup>, <sup>1</sup>H NMR suggests that the produced NH<sub>3</sub> is derived from both N–O reduction and C–N oxidation with their corresponding FE of 72.3% and 52.1%, respectively (Fig. 6c). Based on the quantification of reactants and products, the elemental balance of nitrogen and carbon was 87.8% and 80.0%, respectively (detailed in Fig. S40, ESI†), suggesting that eqn (4) is a reasonable description of the paired process. Considering the abundance of organic Nr in the wastes from certain industries such as meat processing facilities,<sup>36,37</sup> this “one-pot” strategy for converting various Nr into NH<sub>3</sub> not only improves the utilization of electrons, but also mitigates the cost of reactant separation and purification for complex real waste matrices.

## Conclusions

In this work, an integrated sustainable process was presented for economically upcycling waste nitrogen. In particular, a versatile, robust, and inexpensive MFAEL system was developed to convert various forms of waste Nr into NH<sub>3</sub> convergently. Taking advantage of its strong tendency towards hydrogenating N–O bonds, a partial current density as high as 4.22 ± 0.25 A cm<sup>-2</sup> for NH<sub>3</sub> production was achieved by NO<sub>3</sub><sup>-</sup> reduction without generating considerable N–N coupling products.

Upscaling the MFAEL system is straightforward due to its structural simplicity and the inexpensiveness of its components. The 2.5 L scaled-up reactor is capable of producing NH<sub>3</sub> at 25 A with an average FE of 70.4% from NO<sub>3</sub>RR. By properly choosing the NH<sub>3</sub> absorbing conditions, different forms of pure NH<sub>3</sub>-based chemicals (NH<sub>4</sub><sup>+</sup> salts, NH<sub>3</sub> solution, and solid NH<sub>4</sub>HCO<sub>3</sub>) can be continuously produced from the conversion of waste Nr in MFAEL. Since the NH<sub>3</sub> product from MFAEL is in a gas mixture, pure NH<sub>3</sub> gas may also be obtained through established economical gas separation technologies (such as pressure swing adsorption) without the need for additional distillation steps.<sup>38</sup> Use of organic or inorganic additives could increase the co-absorption efficiency of MFAEL-derived NH<sub>3</sub> and waste CO<sub>2</sub>,<sup>39</sup> making it a promising dual-purpose process that fixes waste N and C into one useful chemical product NH<sub>4</sub>HCO<sub>3</sub>. Meanwhile, scale-up issues such as electrolyte mixing and heat management need to be addressed to ensure efficient mass transport and stable operation. In fact, the resemblance of MFAEL configuration to the alkaline water electrolyzers (typically operated at 70–90 °C with 25–35 wt% of KOH solutions<sup>40</sup>) has suggested a clear potential towards commercialization, since the latter has been commercially available for over 50 years.

The feasibility of concentrating NO<sub>3</sub><sup>-</sup> by a low-energy cost electrodialysis process was validated both experimentally and analytically *via* a comprehensive TEA study. Combining NO<sub>3</sub><sup>-</sup> concentration by electrodialysis and its reduction in MFAEL generates a competitive leveled total cost of the waste-derived NH<sub>3</sub> product, largely owing to the remarkably low material cost of the MFAEL system. As illustrated by the TEA results, the



reduction of the cell voltage of NO<sub>3</sub>RR should be the primary focus of future work.

In the present work, Ni was chosen as the electrode material primarily due to its inexpensiveness and its excellent corrosion resistance. Not limited to Ni, other metals such as Co, Ru, and Cu can also serve as the cathode in the KOH/NaOH/H<sub>2</sub>O electrolyte, and their performance comparison under the same test conditions is shown in Fig. S41 (ESI<sup>†</sup>). The development of inexpensive, stable, and more active electrocatalysts should be a synchronous task of reactor optimization.

In the NaOH/KOH/H<sub>2</sub>O electrolyte, C–N bonds in organic Nr compounds can be oxidized to produce NH<sub>3</sub>. By controlling the operating conditions of MFAEL, ~100% recovery of the most common forms of Nr into NH<sub>3</sub> can be realized, making it a sensitive and accurate tool for determining N content in complex real-world samples. Oxidation of C–N bonds results in the production of carboxylic acids as a potentially value-added by-product, and pairing the oxidation of C–N bonds (on anode) with the reduction of N–O bonds (on cathode) in MFAEL leads to a cathodic and anodic FE of 72.3% and 52.1% for NH<sub>3</sub> production at 100 mA cm<sup>-2</sup>, respectively, demonstrating its capability of extracting N element from real waste containing both oxidative and reductive forms of Nr. Notwithstanding the great potential of such a paired process, the quantitative impact of other impurities from real-world feedstocks is subject to further study. In addition, the trade-off between the economic benefits of carboxylic acid products and their separation costs needs to be optimized in future research.

## Author contributions

W. Li and S. Gu proposed and supervised the research. Y. Chen set up the MFAEL system and performed most of the electrochemical measurements. P. Ammari-Azar carried out electro-dialysis experiments. H. Liu carried out the product analysis by HPLC and performed the electrochemical characterization. J. Lee performed SEM and EDS characterization. Y. Xi assisted with the electrochemical measurements. S. Gu performed the techno-economic analysis. M. J. Castellano provided important and constructive suggestions for this work. Y. Chen, S. Gu, and W. Li wrote the manuscript.

## Conflicts of interest

There are no conflicts to declare.

## Acknowledgements

This research was supported by the U.S. National Science Foundation through the Future Manufacturing program (under grant no. CHE-2036944) and the ECO-CBET program (under grants no. 2219162 and 2219172), and by the Regents Innovation Fund of Iowa State Economic Development & Industry Relations. We are grateful to Dr Dapeng Jing for XPS measurements, Jacob F. Wheaton for Raman spectra collection, and

Tianlei Li for assistance in NMR measurements. We thank Dr Zhiyou Wen (Gross-Wen Technologies, Inc.) and Hong Chen for kindly providing the algae powder samples. We also acknowledge fruitful discussions with Peter Hong, Dr Terry A. Houser, Dr Rodrigo Tarté, Dr Joseph G. Sebranek, and Dr Mark M. Wright from Iowa State University on the use of MFAEL for real N-containing wastes. S. Gu acknowledges the John A. See Innovation Foundation. W. Li acknowledges his Herbert L. Stiles Faculty Fellowship and the Presidential Interdisciplinary Research Initiative (PIRI) grant from Iowa State University.

## References

- 1 N. Lehnert, H. T. Dong, J. B. Harland, A. P. Hunt and C. J. White, *Nat. Rev. Chem.*, 2018, **2**, 278–289.
- 2 M. M. M. Kuypers, H. K. Marchant and B. Kartal, *Nat. Rev. Microbiol.*, 2018, **16**, 263–276.
- 3 A. Uwizeye, I. J. M. de Boer, C. I. Opio, R. P. O. Schulte, A. Falcucci, G. Tempio, F. Teillard, F. Casu, M. Rulli, J. N. Galloway, A. Leip, J. W. Erisman, T. P. Robinson, H. Steinfeld and P. J. Gerber, *Nat. Food*, 2020, **1**, 437–446.
- 4 J. N. Galloway and E. B. Cowling, *Ambio*, 2021, **50**, 745–749.
- 5 D. Fowler, M. Coyle, U. Skiba, M. A. Sutton, J. N. Cape, S. Reis, L. J. Sheppard, A. Jenkins, B. Grizzetti, J. N. Galloway, P. Vitousek, A. Leach, A. F. Bouwman, K. Butterbach-Bahl, F. Dentener, D. Stevenson, M. Amann and M. Voss, *Philos. Trans. R. Soc., B*, 2013, **368**, 20130164.
- 6 J. N. Galloway, A. R. Townsend, J. W. Erisman, M. Bekunda, Z. Cai, J. R. Freney, L. A. Martinelli, S. P. Seitzinger and M. A. Sutton, *Science*, 2008, **320**, 889–892.
- 7 J. N. Galloway, J. D. Aber, J. W. Erisman, S. P. Seitzinger, R. W. Howarth, E. B. Cowling and B. J. Cosby, *BioScience*, 2003, **53**, 341–356.
- 8 M. H. Ward, T. M. DeKok, P. Levallois, J. Brender, G. Gulis, B. T. Nolan and J. VanDerslice, *Environ. Health Perspect.*, 2005, **113**, 1607–1614.
- 9 A. Temkin, S. Evans, T. Manidis, C. Campbell and O. V. Naidenko, *Environ. Res.*, 2019, **176**, 108442.
- 10 M. H. Ward, R. R. Jones, J. D. Brender, T. M. de Kok, P. J. Weyer, B. T. Nolan, C. M. Villanueva and S. G. van Breda, *Int. J. Environ. Res. Public Health*, 2018, **15**, 1557.
- 11 Grand Challenges - Introduction to the Grand Challenges for Engineering, <https://www.engineeringchallenges.org/challenges/16091.aspx>, (accessed November 13, 2021).
- 12 P. H. van Langevelde, I. Katsounaros and M. T. M. Koper, *Joule*, 2021, **5**, 290–294.
- 13 J. M. McEnaney, S. J. Blair, A. C. Nielander, J. A. Schwalbe, D. M. Koshy, M. Cargnello and T. F. Jaramillo, *ACS Sustainable Chem. Eng.*, 2020, **8**, 2672–2681.
- 14 X. Deng, Y. Yang, L. Wang, X.-Z. Fu, J.-L. Luo, X. Deng, L. Wang, Z. X. Fu, J.-L. Luo and Y. Yang, *Adv. Sci.*, 2021, **8**, 2004523.
- 15 F.-Y. Chen, Z.-Y. Wu, S. Gupta, D. J. Rivera, S. V. Lambeets, S. Pecaut, J. Y. T. Kim, P. Zhu, Y. Z. Finfrook, D. M. Meira, G. King, G. Gao, W. Xu, D. A. Cullen, H. Zhou, Y. Han,



- D. E. Perea, C. L. Muhich and H. Wang, *Nat. Nanotechnol.*, 2022, **17**, 759–767.
- 16 Q. Hu, Y. Qin, X. Wang, Z. Wang, X. Huang, H. Zheng, K. Gao, H. Yang, P. Zhang, M. Shao and C. He, *Energy Environ. Sci.*, 2021, **14**, 4989–4997.
- 17 Q. Gao, H. S. Pillai, Y. Huang, S. Liu, Q. Mu, X. Han, Z. Yan, H. Zhou, Q. He, H. Xin and H. Zhu, *Nat. Commun.*, 2022, **13**, 2338.
- 18 J. Li, G. Zhan, J. Yang, F. Quan, C. Mao, Y. Liu, B. Wang, F. Lei, L. Li, A. W. M. Chan, L. Xu, Y. Shi, Y. Du, W. Hao, P. K. Wong, J. Wang, S. X. Dou, L. Zhang and J. C. Yu, *J. Am. Chem. Soc.*, 2020, **142**, 7036–7046.
- 19 H. Liu, X. Lang, C. Zhu, J. Timoshenko, M. Rüscher, L. Bai, N. Guijarro, H. Yin, Y. Peng, J. Li, Z. Liu, W. Wang, B. R. Cuenya and J. Luo, *Angew. Chem., Int. Ed.*, 2022, **61**, e202202556.
- 20 S. Licht, B. Cui, B. Wang, F. F. Li, J. Lau and S. Liu, *Science*, 2014, **345**, 637–640.
- 21 S. Licht, B. Cui, B. Wang, F.-F. Li, J. Lau and S. Liu, *Science*, 2020, **369**, 780.
- 22 Y. Chen, H. Liu, N. Ha, S. Licht, S. Gu and W. Li, *Nat. Catal.*, 2020, **3**, 1055–1061.
- 23 G. J. Janz, C. B. Allen, N. P. Bansal, R. M. Murphy and R. P. T. Tomkins, *Physical Properties Data Compilations Relevant to Energy Storage. II. Molten Salts: Data on Single and Multi-Component Salt Systems*, U.S. Government Printing Office, Washington, 1979.
- 24 S. Klaus, Y. Cai, M. W. Louie, L. Trotochaud and A. T. Bell, *J. Phys. Chem. C*, 2015, **119**, 7243–7254.
- 25 J.-M. Ye, D.-H. He, F. Li, Y.-L. Li and J.-B. He, *Chem. Commun.*, 2018, **54**, 10116–10119.
- 26 A. I. Yanson, P. Rodriguez, N. Garcia-Araez, R. V. Mom, F. D. Tichelaar and M. T. M. Koper, *Angew. Chem., Int. Ed.*, 2011, **50**, 6346–6350.
- 27 G. Jeerh, M. Zhang and S. Tao, *J. Mater. Chem. A*, 2021, **9**, 727–752.
- 28 T. Li, E. W. Lees, M. Goldman, D. A. Salvatore, D. M. Weekes and C. P. Berlinguette, *Joule*, 2019, **3**, 1487–1497.
- 29 H. Liu, Y. Chen, J. Lee, S. Gu and W. Li, *ACS Energy Lett.*, 2022, **7**, 4483–4489.
- 30 B. D. James and D. A. DeSantis, *Manufacturing Cost and Installed Price Analysis of Stationary Fuel Cell Systems*, 2015.
- 31 A. Rushing, J. Kneifel and B. Lippiatt, *Energy Price Indices and Discount Factors for Life-Cycle Cost Analysis – 2013*, NIST Interagency/Internal Report (NISTIR), National Institute of Standards and Technology, Gaithersburg, MD, 2013.
- 32 *JJ Environmental, Final Report - Low Cost Retrofits for Nitrogen Removal at Wastewater Treatment Plants in the Upper Long Island Sound Watershed*, 2015.
- 33 E. Pehlivanoglu-Mantas and D. L. Sedlak, *Crit. Rev. Environ. Sci. Technol.*, 2006, **36**, 261–285.
- 34 T. Berman and D. A. Bronk, *Aquat. Microb. Ecol.*, 2003, **31**, 279–305.
- 35 W. M. Haynes, *CRC Handbook of Chemistry and Physics*, CRC Press, 2016.
- 36 C. F. Bustillo-Lecompte and M. Mehrvar, *J. Environ. Manage.*, 2015, **161**, 287–302.
- 37 B. Brennan, J. Lawler and F. Regan, *Environ. Sci.: Water Res. Technol.*, 2021, **7**, 259–273.
- 38 M. Wang, M. A. Khan, I. Mohsin, J. Wicks, A. H. Ip, K. Z. Sumon, C.-T. Dinh, E. H. Sargent, I. D. Gates and M. G. Kibria, *Energy Environ. Sci.*, 2021, **14**, 2535–2548.
- 39 F. Wang, J. Zhao, H. Miao, J. Zhao, H. Zhang, J. Yuan and J. Yan, *Appl. Energy*, 2018, **230**, 734–749.
- 40 N. Guillet and P. Millet, *Hydrogen Prod.*, 2015, 117–166.
- 41 N. W. Rosenberg and C. E. Tirrell, *Ind. Eng. Chem.*, 1957, **49**, 780–784.
- 42 J. M. Baker and T. J. Griffis, *J. Environ. Qual.*, 2017, **46**, 1528–1534.

